Applied Numerical Mathematics 153 (2020) 519–539

Contents lists available at ScienceDirect

Applied Numerical Mathematics

www.elsevier.com/locate/apnum

High-order Runge-Kutta discontinuous Galerkin methods with a new type of multi-resolution WENO limiters on triangular meshes

Jun Zhu [a,1], Chi-Wang Shu [b,2], Jianxian Qiu [c,*,3]

[a] College of Science, Nanjing University of Aeronautics and Astronautics, Nanjing, Jiangsu 210016, PR China
[b] Division of Applied Mathematics, Brown University, Providence, RI 02912, USA
[c] School of Mathematical Sciences and Fujian Provincial Key Laboratory of Mathematical Modeling and High-Performance Scientific Computing, Xiamen University, Xiamen, Fujian 361005, PR China

ARTICLE INFO

Article history:
Received 20 February 2020
Accepted 13 March 2020
Available online 19 March 2020

Keywords:
Runge-Kutta discontinuous Galerkin method
Multi-resolution WENO limiter
Non-oscillatory property
Triangular mesh

ABSTRACT

In this paper, high-order Runge-Kutta discontinuous Galerkin (RKDG) methods with multi-resolution weighted essentially non-oscillatory (WENO) limiters are designed for solving hyperbolic conservation laws on triangular meshes. These multi-resolution WENO limiters are new extensions of the associated multi-resolution WENO finite volume schemes [49,50] which serve as limiters for RKDG methods from structured meshes [47] to triangular meshes. Such new WENO limiters use information of the DG solution essentially only within the troubled cell itself which is identified by a new modified version of the original KXRCF indicator [24], to build a sequence of hierarchical L^2 projection polynomials from zeroth degree to the highest degree of the RKDG method. The second-order, third-order, and fourth-order RKDG methods with associated multi-resolution WENO limiters are developed as examples, which could maintain the original order of accuracy in smooth regions and keep essentially non-oscillatory property near strong shocks or contact discontinuities by gradually degrading from the highest order to the first order. The linear weights inside the procedure of the new multi-resolution WENO limiters can be any positive numbers on the condition that their sum equals one. This is the first time that a series of polynomials of different degrees within the troubled cell itself are applied in a WENO fashion to modify the DG solutions in the troubled cell on triangular meshes. These new WENO limiters are very simple to construct, and can be easily implemented to arbitrary high-order accuracy and in higher dimensions on unstructured meshes. Such spatial reconstruction methodology improves the robustness in the simulation on the same compact spatial stencil of the original DG methods on triangular meshes. Extensive one-dimensional (run as two-dimensional problems on triangular meshes) and two-dimensional tests are performed to demonstrate the effectiveness of these RKDG methods with the new multi-resolution WENO limiters.

* Corresponding author.
E-mail addresses: zhujun@nuaa.edu.cn (J. Zhu), chi-wang_shu@brown.edu (C.-W. Shu), jxqiu@xmu.edu.cn (J. Qiu).

[1] Research was supported by NSFC grant 11872210 and Science Challenge Project, No. TZ2016002. The author was also partly supported by NSFC grant 11826104 when he visited Tianyuan Mathematical Center in Southeast China, Xiamen, Fujian 361005, P.R. China.
[2] Research was supported by NSF grant DMS-1719410.
[3] Research was supported by NSAF grant U1630247 and Science Challenge Project, No. TZ2016002.

https://doi.org/10.1016/j.apnum.2020.03.013
0168-9274/

1. Introduction

In this paper we study two-dimensional conservation laws

$$\begin{cases} u_t + f(u)_x + g(u)_y = 0, \\ u(x, y, 0) = u_0(x, y), \end{cases} \tag{1.1}$$

using the Runge-Kutta discontinuous Galerkin (RKDG) methods [7–9,11] with new multi-resolution WENO limiters on triangular meshes. We apply the DG methods to discretize the spatial variables and adopt explicit, nonlinearly stable high-order Runge-Kutta methods [6,12,21,28,38,40] to discretize the temporal variable. Our objective of this paper is to design a new simple and robust high-order spatial limiting procedure to obtain uniform high-order accuracy in smooth regions and sustain sharp, non-oscillatory shock transitions in non-smooth regions for arbitrary high-order RKDG methods on triangular meshes.

As it is well known, DG methods can be directly applied to compute the numerical solution of (1.1) on the condition that the solution is smooth enough or contains weak discontinuities in the computational field. We first briefly review the development history of the DG methods. In 1973, Reed and Hill [36] proposed the first discontinuous Galerkin (DG) method in the framework of neutron transport. But if problems contain strong discontinuities, the numerical solution has spurious oscillations near these discontinuities and this may lead to nonlinear instability. One common strategy to control these oscillations is to apply nonlinear limiters to RKDG methods. A major development of the DG method with a classical *minmod* type total variation bounded (TVB) limiter was carried out by Cockburn et al. in a series of papers [7–11] to solve nonlinear time dependent hyperbolic conservation laws together with the application of an explicit, nonlinearly stable high-order Runge-Kutta time discretization method [40]. Such methods are termed as RKDG methods. One type of limiters is based on slope modification, such as above mentioned *minmod* type limiters [7–9,11], the moment based limiter [1], and an improved moment limiter [3], etc. Such limiters belong to the slope type limiters and they could suppress spurious oscillations at the price of possibly degrading the numerical accuracy at smooth extrema. Another type of limiters is based on the weighted essentially non-oscillatory (WENO) methodology [14,22,23,29,37], which can achieve high-order accuracy in smooth regions and keep the essentially non-oscillatory property near strong discontinuities. The WENO limiters [30,33,34,48] and Hermite WENO limiters [30–32,35] belong to the second type of limiters. These limiters are designed in a finite volume WENO fashion, but they need a wider spatial stencil for obtaining high-order schemes. Therefore, it is difficult to implement them for multi-dimensional problems, especially on triangular meshes or tetrahedral meshes.

Recently, a new type of multi-resolution finite difference or finite volume WENO schemes is designed in [49–51] for solving hyperbolic conservation laws, in which only the information defined on a hierarchy of nested central spatial stencils is used and no equivalent multi-resolution representation [16–20] is introduced. These new WENO schemes adopt the same large stencils as that of the classical WENO schemes in [23,39] on structured meshes, could obtain the optimal order of accuracy in smooth regions, and could gradually degrade from the optimal order to first order accuracy near strong shocks or contact discontinuities. The linear weights of them can be any positive numbers on the condition that their sum is one. In [47], we adapted this new class of multi-resolution WENO schemes as limiters for high-order RKDG methods on structured meshes. In this paper, as a continuation of [47], we extend this new multi-resolution WENO limiter for high-order RKDG methods to unstructured triangular meshes. Two major advantages of these multi-resolution WENO limiters are the compactness of their spatial stencil, which essentially only contain the triangular troubled cell itself with information from neighboring triangular cells used only to determine the smoothness indicator of the zeroth degree polynomial in the hierarchy, and the simplicity in implementation. In order to keep the advantages of the compact stencil and simplicity of linear weights, we make a small modification of the procedure in [49], using orthogonal basis and L^2 projection to define the sequence of hierarchical polynomials of different degrees in the triangular troubled cell. This modification facilitates the achievement of strict conservation and the maintenance of as much information of the original polynomial in the triangular troubled cell as possible through the mechanism of a gradual degradation to lower degree polynomials in a L^2 projection fashion with the spatial WENO procedure. Numerical experiments indicate the good behavior of the resulting scheme in its robustness and sharp shock transition.

This paper is organized as follows. In section 2, we briefly review the RKDG methods for solving (1.1) on triangular meshes. In section 3, we present the details of the new multi-resolution WENO procedure for two-dimensional scalar and system problems on triangular meshes. Numerical examples are provided in section 4 to verify the compactness, accuracy, and stability of this new approach. Concluding remarks are given in section 5.

2. Review of the RKDG method on triangular meshes

This section provides a brief review of the RKDG methods for solving two-dimensional hyperbolic conservation laws (1.1) on triangular meshes.

We first use DG methods to discretize the spatial variables. Given a triangulation of the computational domain consisting of cells $\triangle_j$, the DG method has its solution as well as the test function space given by $V_h^k = \{v(x, y) : v(x, y)|_{\triangle_j} \in \mathbb{P}^k(\triangle_j)\}$, where $\mathbb{P}^k(\triangle_j)$ denotes the set of polynomials of degree at most k defined on $\triangle_j$. The semi-discrete DG method for solving (1.1) is defined as follows. We find the function $u_h \in V_h^k$, such that

$$\int_{\triangle_0} (u_h)_t v \, dx dy = \int_{\triangle_0} \left(f(u_h) v_x + g(u_h) v_y \right) dx dy - \int_{\partial \triangle_0} (f(u^h), g(u^h)) \cdot n \, v \, ds, \tag{2.1}$$

holds for all test functions $v \in V_h^k$. Here $n = (n_x, n_y)^T$ is an outward unit normal of the triangle boundary $\partial\triangle_0$, $(f(u^h), g(u^h)) \cdot n$ is a monotone numerical flux for the scalar case and an exact or approximate Riemann solver for the system case, and v in the last integral over $\partial\triangle_0$ is taken from inside the cell $\triangle_0$. The Lax-Friedrichs flux is used in this paper. For time discretization procedure, a classical third-order Runge-Kutta time discretization method [40]

$$\begin{aligned} u^{(1)} &= u^n + \Delta t L(u^n), \\ u^{(2)} &= \frac{3}{4}u^n + \frac{1}{4}u^{(1)} + \frac{1}{4}\Delta t L(u^{(1)}), \\ u^{n+1} &= \frac{1}{3}u^n + \frac{2}{3}u^{(2)} + \frac{2}{3}\Delta t L(u^{(2)}), \end{aligned} \tag{2.2}$$

is applied to obtain a fully discrete scheme both in space and in time.

3. Multi-resolution WENO limiter on triangular meshes

In this section, we focus on designing a new multi-resolution WENO reconstruction procedure as a limiter for the second-order, third-order, and fourth-order RKDG methods on triangular meshes. It is an extension to triangular meshes of high-order limiting procedure that was developed in [47] on structured meshes. The main framework of the new multi-resolution WENO limiting procedure on triangular cell is narrated in the following.

3.1. A new modified KXRCF shock detection technique

One crucial objective of this subsection is to identify the troubled cells precisely, namely those triangular cells which may need the new multi-resolution WENO limiting procedure later. This is important for limiters. If excessive triangular cells are identified as troubled cells, the computational cost will increase greatly. If too few triangular cells are identified as troubled cells, the spurious oscillations may appear in non-smooth regions and the codes may stop computing for the appearance of negative density, negative pressure, or negative energy, etc. A comparison among different troubled cell indicators is given in [34]. The classical KXRCF shock detection technique [24] is widely used in detecting troubled cells, which are cells that may contain strong shocks or contact discontinuities and in which the multi-resolution WENO limiter is applied. We propose a new modified version of the classical KXRCF shock detection technique [24] to detect troubled cells on triangular meshes. Other troubled cell detectors can of course also be used, but our emphasis in this paper is not to study the pros and cons of various troubled cell indicators. As shown in [24], we will divide the boundary of the triangular cell Δ_j into two parts: $\partial\Delta_j^-$ and $\partial\Delta_j^+$, where the flow is into and out of Δ_j, respectively. In the one-dimensional case, Fu and Shu [15] noted that the scaling of $|x_{j+\frac{1}{2}} - x_{j-\frac{1}{2}}|^{\frac{k+1}{2}}$ tends to mark a lot more troubled cells than necessary for high-order DG methods. They decreased the power of $|x_{j+\frac{1}{2}} - x_{j-\frac{1}{2}}|$ to be $\frac{\min(k,2)+1}{2}$, which seems to be strong enough to single out discontinuities [15]. Now on triangular meshes, we define the triangular cell Δ_0 as a troubled cell on the condition that

$$\frac{|\int_{\partial\Delta_0^-}(u_h(x,y,t)|_{\Delta_0} - u_h(x,y,t)|_{\Delta_l})ds|}{h_0^R |\partial\Delta_0^-| \cdot |||\widehat{u_h}(x,y,t)|_{\partial\Delta_0}|||} \geq C_k, \tag{3.1}$$

where $R = 1$ for $k = 1$ and $R = 1.5$ for $k > 1$, h_0 is the radius of the circumscribed circle in the triangular cell Δ_0, and C_k is a constant, usually, we take $C_k = 1$ as specified in [24]. Here Δ_l, $l = 1, 2, 3$ (as shown in Fig. 3.1) denote the neighboring triangular cells of Δ_0 on the side of $\partial\Delta_0^-$. $u_h(x, y, t)$ is the numerical solution corresponding to the indicator variable(s) and $|||\widehat{u_h}(x, y, t)|_{\partial\Delta_0}|||$ is defined as the minimum value of $|u_h(x, y, t)|$ along $\partial\Delta_0$. By using (3.1), we do not need to adopt different types of C_k to compute multi-dimensional test problems as in [15] and can simply set $C_k = 1$ in all numerical computations, unless specified otherwise. This new modified KXRCF shock detection technique is simple and robust enough to catch strong discontinuities without identifying excessive troubled cells on triangular meshes.

3.2. New multi-resolution WENO limiting procedure

The objective of this subsection is to reconstruct a new polynomial using the multi-resolution WENO limiting procedure to replace the solution polynomial on the troubled cell. The new polynomial should maintain the cell average and high-order accuracy of the original DG solution without introducing oscillations on triangular meshes.

First, the details of the new multi-resolution WENO limiting procedure are presented for the scalar case. The basic idea is to reconstruct a new polynomial on the troubled cell $I_{i,j}$ which is a convex combination of polynomials of different degrees: the DG solution polynomial on this triangular cell and a sequence of hierarchical "modified" solution polynomials based on

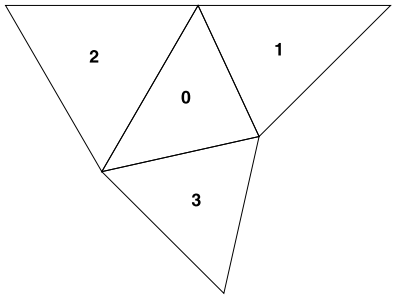

Fig. 3.1. $\triangle_0$ and its neighboring triangular cells $\triangle_1$, $\triangle_2$, and $\triangle_3$.

the L^2 projection methodology. The nonlinear weights in the convex combination coefficients follow the standard WENO procedure. For simplicity, we also rewrite $u_h(x, y, t)$ to be $u_h(x, y) \in W_h^k = \{v(x, y) : v(x, y)|_{\Delta_0} \in \mathbb{P}^k(\Delta_0)\}$ in the following, if it does not cause confusion. Now we assume Δ_0 is a troubled cell which is detected by our new proposed troubled cell indicator. The procedure to reconstruct a new polynomial on the troubled cell Δ_0 by using the new multi-resolution WENO reconstruction procedure is summarized as follows:

Step 1.1. Define a series of polynomials of different degrees on the troubled cell Δ_0. We construct polynomials $q_\ell(x, y), \ell = 0, ..., k$, which satisfy

$$\int_{\Delta_0} q_\ell(x, y) v_l^{(0)}(x, y) dxdy = \int_{\Delta_0} u_h(x, y) v_l^{(0)}(x, y) dxdy, \ l = 0, ..., \frac{(\ell+1)(\ell+2)}{2} - 1. \tag{3.2}$$

Remark 1. The construction of different polynomials $q_\ell(x, y), \ell = 0, ..., k$ is very simple, if we adopt local orthonormal basis $v_l^{(0)}(x, y)$ over Δ_0. In this case, we can directly obtain $q_\ell(x, y) = \sum_{l=0}^{\frac{(\ell+1)(\ell+2)}{2}-1} u_0^{(l)}(t) v_l^{(0)}(x, y), \ell = 0, ..., k$, respectively.

Step 1.2. Obtain equivalent expressions for these constructed polynomials of different degrees. To keep consistent notation, we will denote $p_{0,1}(x, y) = q_0(x, y)$. For different high-order approximations, following similar ideas for classical CWENO schemes [4,26,27] and in [45,46], we obtain polynomials $p_{\ell,\ell}(x, y), \ \ell = 1, ..., k$ through

$$p_{\ell,\ell}(x, y) = \frac{1}{\gamma_{\ell,\ell}} q_\ell(x, y) - \frac{\gamma_{\ell-1,\ell}}{\gamma_{\ell,\ell}} p_{\ell-1,\ell}(x, y), \ \ell = 1, ..., k, \tag{3.3}$$

with $\gamma_{\ell-1,\ell} + \gamma_{\ell,\ell} = 1$ and $\gamma_{\ell,\ell} \neq 0$, together with polynomials $p_{\ell,\ell+1}(x, y), \ \ell = 1, ..., k-1$ through

$$p_{\ell,\ell+1}(x, y) = \omega_{\ell,\ell} p_{\ell,\ell}(x, y) + \omega_{\ell-1,\ell} p_{\ell-1,\ell}(x, y), \ell = 1, ..., k-1, \tag{3.4}$$

with $\omega_{\ell-1,\ell} + \omega_{\ell,\ell} = 1$. In these expressions, $\gamma_{\ell-1,\ell}$ and $\gamma_{\ell,\ell}$ are the linear weights, and $\omega_{\ell-1,\ell}$ and $\omega_{\ell,\ell}$ are the nonlinear weights (which will be precisely narrated later), respectively. Based on a balance between the sharp and essentially non-oscillatory shock transitions in non-smooth regions and accuracy in smooth regions, following the practice in [13,44–46,52], we set the linear weights as $\gamma_{\ell-1,\ell} = 0.01$ and $\gamma_{\ell,\ell} = 0.99$, $\ell = 1, ..., k$, respectively.

Step 1.3. Compute the smoothness indicators β_{ℓ,ℓ_2}, which measure how smooth the functions $p_{\ell,\ell_2}(x, y)$ for $\ell = \ell_2 - 1, \ell_2$; $\ell_2 = 1, 2, 3$ are in the triangular cell Δ_0. We use the same recipe for the smoothness indicators as in [23,39]:

$$\beta_{\ell,\ell_2} = \sum_{|\alpha|=1}^{\kappa} \int_{\Delta_0} \Delta_0^{|\alpha|-1} \left(\frac{\partial^{|\alpha|}}{\partial x^{\alpha_1} \partial y^{\alpha_2}} p_{\ell,\ell_2}(x, y) \right)^2 dxdy, \ \ell = \ell_2 - 1, \ell_2; \ \ell_2 = 1, 2, 3, \tag{3.5}$$

where $\kappa = \ell$, $\alpha = (\alpha_1, \alpha_2)$, and $|\alpha| = \alpha_1 + \alpha_2$, respectively. The only exception is $\beta_{0,1}$, which we magnify from zero to a value defined below. As shown in Fig. 3.1, we first denote the linear polynomial $q_{0,1}(x, y)$ with the L^2 projection methodology of $u_h(x, y) \in W_h^k = \{v(x, y) : v(x, y)|_{\Delta_1} \in \mathbb{P}^k(\Delta_1)\}$ satisfying

$$\int_{\Delta_1} q_{0,1}(x, y) v_l^{(1)}(x, y) dxdy = \int_{\Delta_1} u_h(x, y) v_l^{(1)}(x, y) dxdy, \ l = 0, 1, 2, \tag{3.6}$$

the linear polynomial $q_{0,2}(x, y)$ with the L^2 projection methodology of $u_h(x, y) \in W_h^k = \{v(x, y) : v(x, y)|_{\Delta_2} \in \mathbb{P}^k(\Delta_2)\}$ satisfying

$$\int_{\Delta_2} q_{0,2}(x, y) v_l^{(2)}(x, y) dxdy = \int_{\Delta_2} u_h(x, y) v_l^{(2)}(x, y) dxdy, \ l = 0, 1, 2, \tag{3.7}$$

and the linear polynomial $q_{0,3}(x,y)$ with the L^2 projection methodology of $u_h(x,y)\in W_h^k=\{v(x,y):v(x,y)|_{\Delta_3}\in\mathbb{P}^k(\Delta_3)\}$ satisfying

$$\int_{\Delta_3} q_{0,3}(x,y)v_l^{(3)}(x,y)dxdy=\int_{\Delta_3} u_h(x,y)v_l^{(3)}(x,y)dxdy,\ l=0,1,2. \tag{3.8}$$

Remark 2. We can obtain $q_{0,1}(x,y)=\sum_{l=0}^{2}u_1^{(l)}(t)v_l^{(1)}(x,y)$, $q_{0,2}(x,y)=\sum_{l=0}^{2}u_2^{(l)}(t)v_l^{(2)}(x,y)$, and $q_{0,3}(x,y)=\sum_{l=0}^{2}u_3^{(l)}(t)v_l^{(3)}(x,y)$, respectively.

Then the associated smoothness indicators are

$$\varsigma_{0,1}=\int_{\Delta_0}\left(\frac{\partial}{\partial x}q_{0,1}(x,y)\right)^2+\left(\frac{\partial}{\partial y}q_{0,1}(x,y)\right)^2dxdy, \tag{3.9}$$

$$\varsigma_{0,2}=\int_{\Delta_0}\left(\frac{\partial}{\partial x}q_{0,2}(x,y)\right)^2+\left(\frac{\partial}{\partial y}q_{0,2}(x,y)\right)^2dxdy, \tag{3.10}$$

and

$$\varsigma_{0,3}=\int_{\Delta_0}\left(\frac{\partial}{\partial x}q_{0,3}(x,y)\right)^2+\left(\frac{\partial}{\partial y}q_{0,3}(x,y)\right)^2dxdy. \tag{3.11}$$

After that, we define $\beta_{0,1}$ as

$$\beta_{0,1}=\min(\varsigma_{0,1},\varsigma_{0,2},\varsigma_{0,3}). \tag{3.12}$$

Step 1.4. Compute the nonlinear weights based on the linear weights and the smoothness indicators. We adopt the WENO-Z recipe as shown in [2,5], with τ_{ℓ_2} for $\ell_2=1,2,3$ defined as related to the absolute difference between the smoothness indicators:

$$\tau_{\ell_2}=\left(\beta_{\ell_2,\ell_2}-\beta_{\ell_2-1,\ell_2}\right)^2,\quad \ell_2=1,2,3. \tag{3.13}$$

The nonlinear weights are then given as

$$\omega_{\ell_1,\ell_2}=\frac{\bar{\omega}_{\ell_1,\ell_2}}{\sum_{\ell=\ell_2-1}^{\ell_2}\bar{\omega}_{\ell,\ell_2}},\ \bar{\omega}_{\ell_1,\ell_2}=\gamma_{\ell_1,\ell_2}\left(1+\frac{\tau_{\ell_2}}{\varepsilon+\beta_{\ell_1,\ell_2}}\right),\ \ell_1=\ell_2-1,\ell_2;\ \ell_2=1,2,3. \tag{3.14}$$

Here ε is taken as 10^{-6} in all numerical simulations.

Step 1.5. The new final reconstruction polynomial $u_h^{new}|_{\Delta_0}=p^{new}(x,y)$ on the troubled cell Δ_0 is given by

$$p^{new}(x,y)=\sum_{\ell=\ell_2-1}^{\ell_2}\omega_{\ell,\ell_2}p_{\ell,\ell_2}(x,y),\ \ \ell_2=1,2,3, \tag{3.15}$$

for the second-order, third-order, and fourth-order approximations, respectively.

Thereafter, the details of the new multi-resolution WENO limiting procedure are presented for the systems case. Now we study equation (1.1), where u, $f(u)$, and $g(u)$ are vectors with m components. For the purpose of achieving better non-oscillatory property, the new multi-resolution WENO reconstruction limiter is used with a local characteristic decomposition [37]. In this paper, we only consider the two-dimensional Euler equations and set $m=4$.

$$u_t+f(u)_x+g(u)_y=\frac{\partial}{\partial t}\begin{pmatrix}\rho\\ \rho\mu\\ \rho\nu\\ E\end{pmatrix}+\frac{\partial}{\partial x}\begin{pmatrix}\rho\mu\\ \rho\mu^2+p\\ \rho\mu\nu\\ \mu(E+p)\end{pmatrix}+\frac{\partial}{\partial y}\begin{pmatrix}\rho\nu\\ \rho\mu\nu\\ \rho\nu^2+p\\ \nu(E+p)\end{pmatrix}=0, \tag{3.16}$$

with $u(x,y,0)=u_0(x,y)$, where ρ is the density, μ is the x-direction velocity, ν is the y-direction velocity, E is the total energy, $p=\frac{E}{\gamma-1}-\frac{1}{2}\rho(\mu^2+\nu^2)$ is the pressure, and $\gamma=1.4$, respectively. We denote the Jacobian matrices as $(f'(u),g'(u))\cdot n_i$ and $n_i=(n_{ix},n_{iy})^T$, $i=1,2,3$, are the outward unit normals to different edges of the target cell. We then give the left and right eigenvectors of such Jacobian matrices as specified in [53]. Assuming $\triangle_0$ is the troubled cell detected by the new modified version of original KXRCF technique [24], we denote associated polynomial vectors p_0, p_1, p_2, and p_3, respectively, on the troubled cell. We then perform the new multi-resolution WENO limiting procedure as follows:

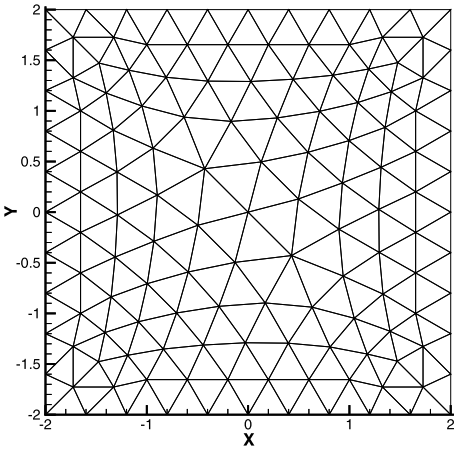

Fig. 4.1. Burgers' equation. Sample mesh.

Table 4.1
$u_t + \left(\frac{u^2}{2}\right)_x + \left(\frac{u^2}{2}\right)_y = 0$. $u(x, y, 0) = 0.5 + \sin(\pi(x+y)/2)$. Periodic boundary conditions in both directions. $T = 0.5/\pi$. L^1, L^∞, and L^2 errors.

		RKDG with new multi-resolution WENO limiter						RKDG without limiter					
	cell	L^1 error	order	L^∞ error	order	L^2 error	order	L^1 error	order	L^∞ error	order	L^2 error	order
P^1	232	1.56E-2		1.89E-1		2.23E-2		1.43E-2		1.06E-1		2.07E-2	
	928	3.52E-3	2.15	2.88E-2	2.71	5.35E-3	2.06	3.54E-3	2.01	2.92E-2	1.86	5.38E-3	1.94
	3712	8.67E-4	2.02	7.78E-3	1.89	1.36E-3	1.97	8.68E-4	2.02	7.79E-3	1.91	1.36E-3	1.98
	14848	2.15E-4	2.01	2.13E-3	1.87	3.45E-4	1.98	2.15E-4	2.01	2.13E-3	1.87	3.45E-4	1.98
	59392	5.36E-5	2.00	5.58E-4	1.93	8.70E-5	1.99	5.36E-5	2.00	5.58E-4	1.93	8.70E-5	1.99
P^2	232	2.40E-3		2.26E-2		3.81E-3		1.92E-3		2.27E-2		3.16E-3	
	928	3.10E-4	2.95	4.33E-3	2.39	5.39E-4	2.82	2.98E-4	2.69	4.33E-3	2.39	5.16E-4	2.61
	3712	4.22E-5	2.88	7.58E-4	2.52	7.96E-5	2.76	4.23E-5	2.81	7.58E-4	2.52	7.96E-5	2.70
	14848	5.70E-6	2.89	1.18E-4	2.68	1.15E-5	2.79	5.70E-6	2.89	1.18E-4	2.68	1.15E-5	2.79
	59392	7.67E-7	2.89	1.77E-5	2.73	1.63E-6	2.82	7.67E-7	2.89	1.77E-5	2.73	1.63E-6	2.82
P^3	232	3.38E-4		5.24E-3		7.49E-4		3.07E-4		5.40E-3		7.04E-4	
	928	2.20E-5	3.94	5.46E-4	3.26	5.88E-5	3.67	2.20E-5	3.80	5.46E-4	3.31	5.88E-5	3.58
	3712	1.28E-6	4.10	3.91E-5	3.80	3.64E-6	4.01	1.28E-6	4.10	3.91E-5	3.80	3.64E-6	4.01
	14848	8.01E-8	4.00	2.59E-6	3.91	2.28E-7	4.00	8.01E-8	4.00	2.59E-6	3.91	2.28E-7	4.00
	59392	5.14E-9	3.96	1.73E-7	3.90	1.46E-8	3.96	5.14E-9	3.96	1.73E-7	3.90	1.46E-8	3.96

Step 2.1. In each n_i-direction among three normal directions of $\partial\triangle_0$, we reconstruct new polynomial vectors p_i^{new}, $i = 1, 2, 3$, by using the characteristic-wise new multi-resolution WENO limiting procedure with the associated Jacobian $f'(u)n_{ix} + g'(u)n_{iy}$, $i = 1, 2, 3$ as specified in [53]:

Step 2.1.1. Project the polynomial vectors p_0, p_1, p_2, and p_3 into the characteristic fields $\tilde{\tilde{p}}_{i_l} = L_i \cdot p_l$, $i = 1, 2, 3$, $l = 0, 1, 2, 3$. $\tilde{\tilde{p}}_{i_l}$ is a 4-component vector with each component being a polynomial of degree up to k.

Step 2.1.2. For each component of $\tilde{\tilde{p}}_{i_l}$, we perform Step 1.1 to Step 1.5 of the new multi-resolution WENO limiting procedure that has been specified for the scalar case, to obtain new 4-component vectors on the troubled cell $\triangle_0$ as $\tilde{\tilde{p}}_i^{new}$, $i = 1, 2, 3$, respectively.

Step 2.1.3. Project $\tilde{\tilde{p}}_i^{new}$ into the physical space $p_i^{new} = R_i \cdot \tilde{\tilde{p}}_i^{new}$, $i = 1, 2, 3$.

Step 2.2. The final new 4-component vector on the troubled cell $\triangle_0$ is defined as

$$p^{new} = \frac{\sum_{i=1}^{3} p_i^{new} |\triangle_i|}{\sum_{i=1}^{3} |\triangle_i|}.$$

4. Numerical results

In this section, we provide numerical results to testify the performance of the new multi-resolution WENO limiters for the RKDG methods on triangular meshes described in previous sections. For all of our accuracy tests, the refinement is performed by a structured refinement (each triangle is divided into four similar smaller triangles for every level of the refinement). The CFL number is 0.3 for the second-order (P^1), 0.18 for the third-order (P^2), and 0.1 for the fourth-order (P^3) RKDG methods with and without new multi-resolution WENO limiters on triangular meshes, except for the accuracy

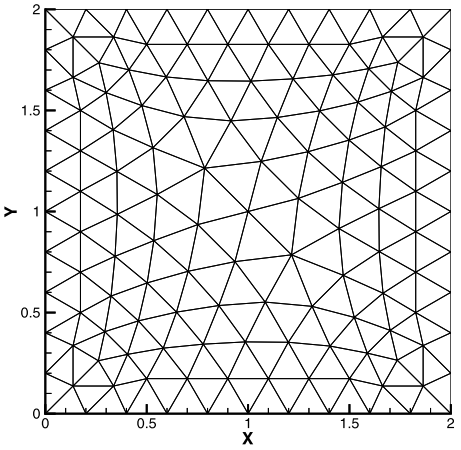

Fig. 4.2. 2D-Euler equations. Sample mesh.

Table 4.2
2D-Euler equations: initial data $\rho(x, y, 0) = 1 + 0.2\sin(\pi(x + y))$, $u(x, y, 0) = 0.7$, $v(x, y, 0) = 0.3$, and $p(x, y, 0) = 1$. Periodic boundary conditions in both directions. $T = 2.0$. L^1, L^∞, and L^2 errors.

		RKDG with new multi-resolution WENO limiter						RKDG without limiter					
	cell	L^1 error	order	L^∞ error	order	L^2 error	order	L^1 error	order	L^∞ error	order	L^2 error	order
P^1	232	3.62E-3		1.60E-2		4.59E-3		3.62E-3		1.60E-2		4.59E-3	
	928	6.51E-4	2.48	3.46E-3	2.22	8.68E-4	2.40	6.51E-4	2.48	3.46E-3	2.22	8.68E-4	2.40
	3712	1.45E-4	2.17	8.68E-4	1.99	1.98E-4	2.13	1.45E-4	2.17	8.68E-4	1.99	1.98E-4	2.13
	14848	3.47E-5	2.06	2.21E-4	1.97	4.77E-5	2.05	3.47E-5	2.06	2.21E-4	1.97	4.77E-5	2.05
	59392	8.53E-6	2.03	5.61E-5	1.98	1.17E-5	2.02	8.53E-6	2.03	5.61E-5	1.98	1.17E-5	2.02
P^2	232	4.84E-4		3.73E-3		6.91E-4		3.36E-4		2.35E-3		4.44E-4	
	928	4.42E-5	3.45	3.45E-4	3.44	5.92E-5	3.54	4.32E-5	2.96	3.38E-4	2.80	5.74E-5	2.95
	3712	5.10E-6	3.12	3.63E-5	3.25	6.70E-6	3.14	5.10E-6	3.08	3.63E-5	3.22	6.70E-6	3.09
	14848	5.96E-7	3.09	4.56E-6	2.99	7.89E-7	3.08	5.96E-7	3.09	4.56E-6	2.99	7.89E-7	3.08
	59392	7.16E-8	3.06	5.63E-7	3.02	9.58E-8	3.04	7.16E-8	3.06	5.63E-7	3.02	9.58E-8	3.04
P^3	232	1.07E-5		8.42E-5		1.51E-5		1.07E-5		8.42E-5		1.51E-5	
	928	5.79E-7	4.22	5.89E-6	3.84	8.47E-7	4.16	5.79E-7	4.22	5.89E-6	3.84	8.47E-7	4.16
	3712	3.41E-8	4.08	3.93E-7	3.91	5.14E-8	4.04	3.41E-8	4.08	3.93E-7	3.91	5.14E-8	4.04
	14848	2.06E-9	4.05	2.20E-8	4.15	3.15E-9	4.03	2.06E-9	4.05	2.20E-8	4.15	3.15E-9	4.03
	59392	1.27E-10	4.02	1.51E-9	3.86	1.95E-10	4.01	1.27E-10	4.02	1.51E-9	3.86	1.95E-10	4.01

Table 4.3
The Lax problem. The maximum and average percentages of troubled cells subject to the new multi-resolution WENO limiting.

Percentage of the troubled cells								
P^1	cell length h	1/200	P^2	cell length h	1/200	P^3	cell length h	1/200
	maximum percent	2.97		maximum percent	6.56		maximum percent	7.65
	average percent	2.09		average percent	4.95		average percent	5.08

Table 4.4
The Sod problem. The maximum and average percentages of troubled cells subject to the new multi-resolution WENO limiting.

Percentage of the troubled cells								
P^1	cell length h	10/200	P^2	cell length h	10/200	P^3	cell length h	10/200
	maximum percent	0.35		maximum percent	1.92		maximum percent	1.22
	average percent	0.03		average percent	1.00		average percent	0.75

Table 4.5
The shock density wave interaction problem. The maximum and average percentages of troubled cells subject to the new multi-resolution WENO limiting.

Percentage of the troubled cells								
P^1	cell length h	10/200	P^2	cell length h	10/200	P^3	cell length h	10/200
	maximum percent	0.99		maximum percent	1.40		maximum percent	1.05
	average percent	0.60		average percent	0.75		average percent	0.57

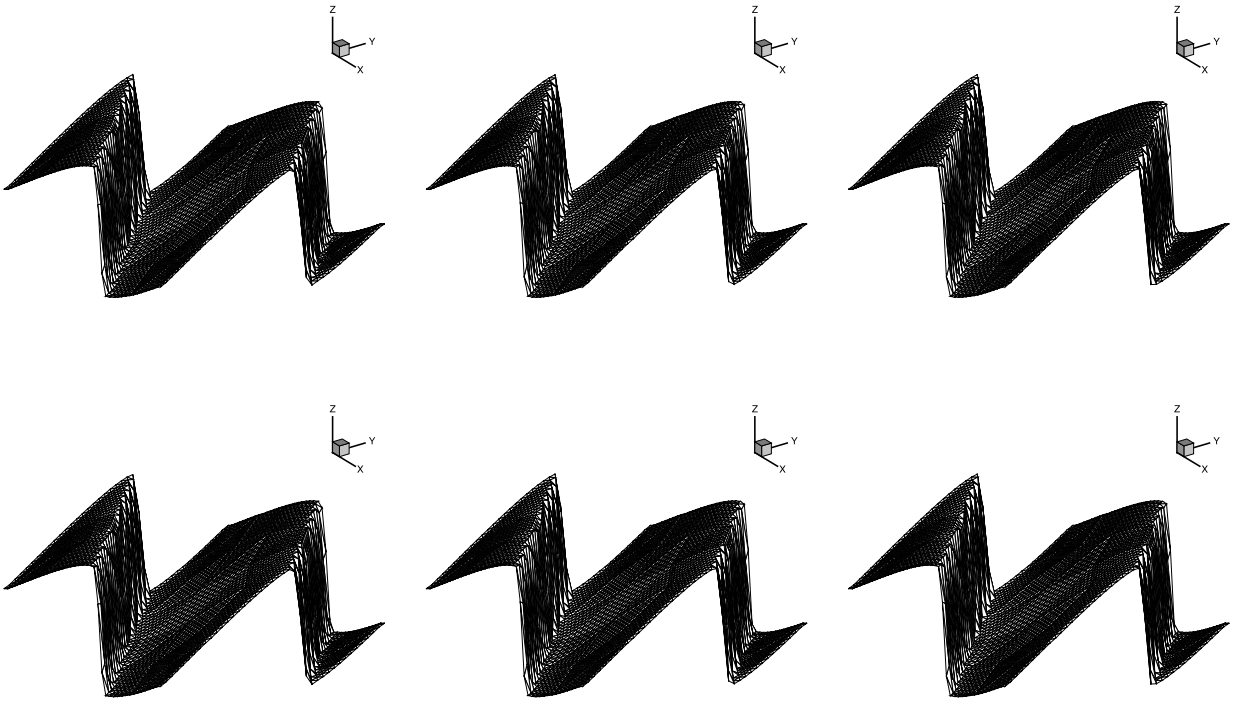

Fig. 4.3. Burgers' equation. $T = 1.5/\pi$. The surface of the solution. RKDG with new multi-resolution WENO limiter. Top: $C_k = 1$; bottom: all cells are defined as troubled cells. Left: second-order ($k = 1$); middle: third-order ($k = 2$); right: fourth-order ($k = 3$).

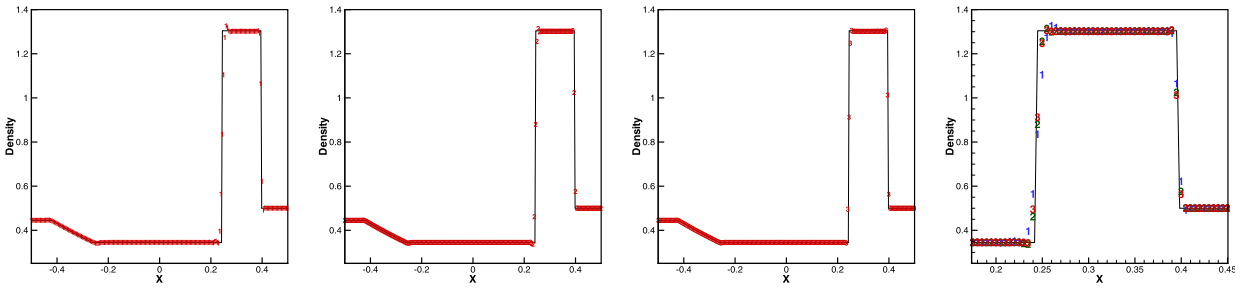

Fig. 4.4. The Lax problem. $T = 0.16$. Density cut at $y = 0$. Solid line: the exact solution; numbers: RKDG with new multi-resolution WENO limiter. From left to right: "1" for second-order ($k = 1$); "2" for third-order ($k = 2$); "3" for fourth-order ($k = 3$); density zoomed-in. The mesh points on the boundary are uniformly distributed with cell length $h = 1/200$.

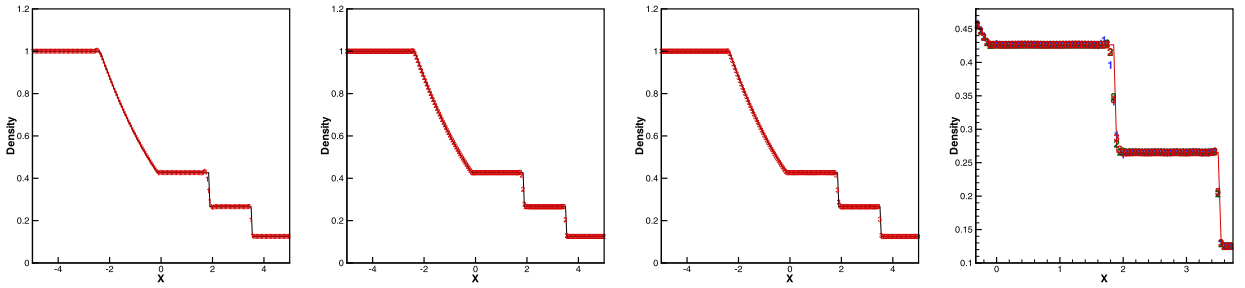

Fig. 4.5. The Sod problem. $T = 2$. Density cut at $y = 0$. Solid line: the exact solution; numbers: RKDG with new multi-resolution WENO limiter. From left to right: "1" for second-order ($k = 1$); "2" for third-order ($k = 2$); "3" for fourth-order ($k = 3$); density zoomed-in. The mesh points on the boundary are uniformly distributed with cell length $h = 10/200$.

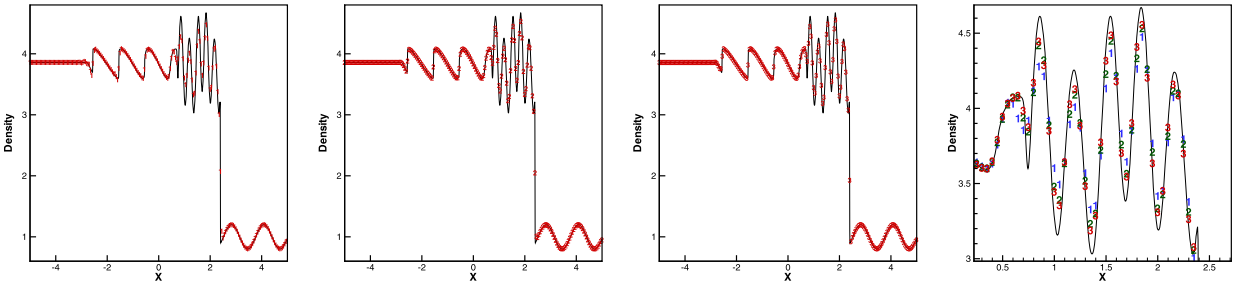

Fig. 4.6. The shock density wave interaction problem. $T = 1.8$. Density cut at $y = 0$. Solid line: the "exact" solution; numbers: RKDG with new multi-resolution WENO limiter. From left to right: "1" for second-order ($k = 1$); "2" for third-order ($k = 2$); "3" for fourth-order ($k = 3$); density zoomed-in. The mesh points on the boundary are uniformly distributed with cell length $h = 10/200$.

Table 4.6
The blast wave problem. The maximum and average percentages of troubled cells subject to the new multi-resolution WENO limiting.

Percentage of the troubled cells								
P^1	cell length h	1/400	P^2	cell length h	1/400	P^3	cell length h	1/400
	maximum percent	2.72		maximum percent	3.46		maximum percent	3.26
	average percent	1.70		average percent	2.58		average percent	1.98

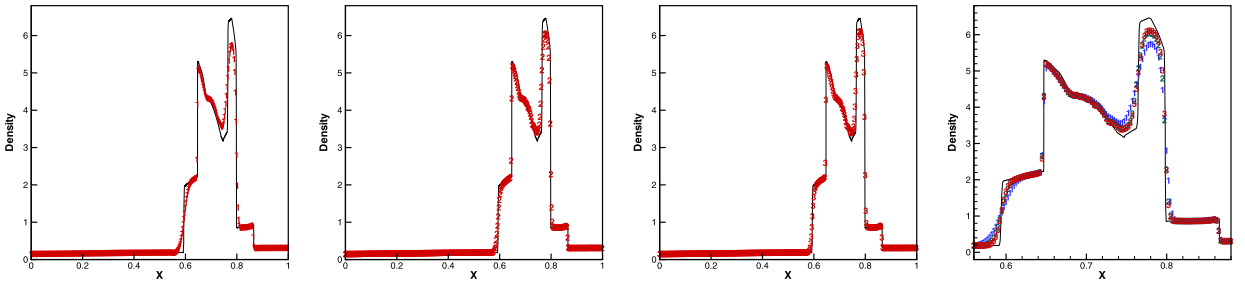

Fig. 4.7. The blast wave problem. T=0.038. Density cut at $y = 0$. Solid line: the "exact" solution; numbers: RKDG with new multi-resolution WENO limiter. From left to right: "1" for second-order ($k = 1$); "2" for third-order ($k = 2$); "3" for fourth-order ($k = 3$); density zoomed-in. The mesh points on the boundary are uniformly distributed with cell length $h = 1/400$.

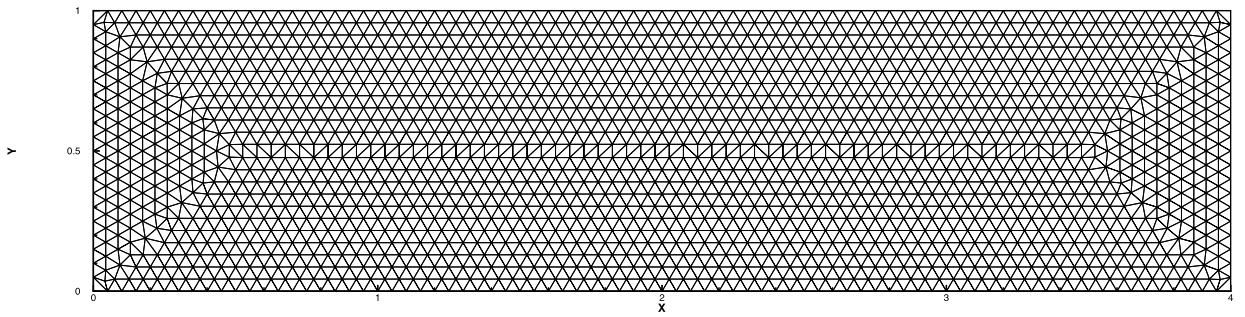

Fig. 4.8. Double Mach reflection problem. Sample mesh.

Table 4.7
Double Mach reflection problem. The maximum and average percentages of troubled cells subject to the new multi-resolution WENO limiting.

Percentage of the troubled cells								
P^1	cell length h	1/200	P^2	cell length h	1/200	P^3	cell length h	1/200
	maximum percent	1.95		maximum percent	6.95		maximum percent	6.95
	average percent	1.31		average percent	3.85		average percent	3.84

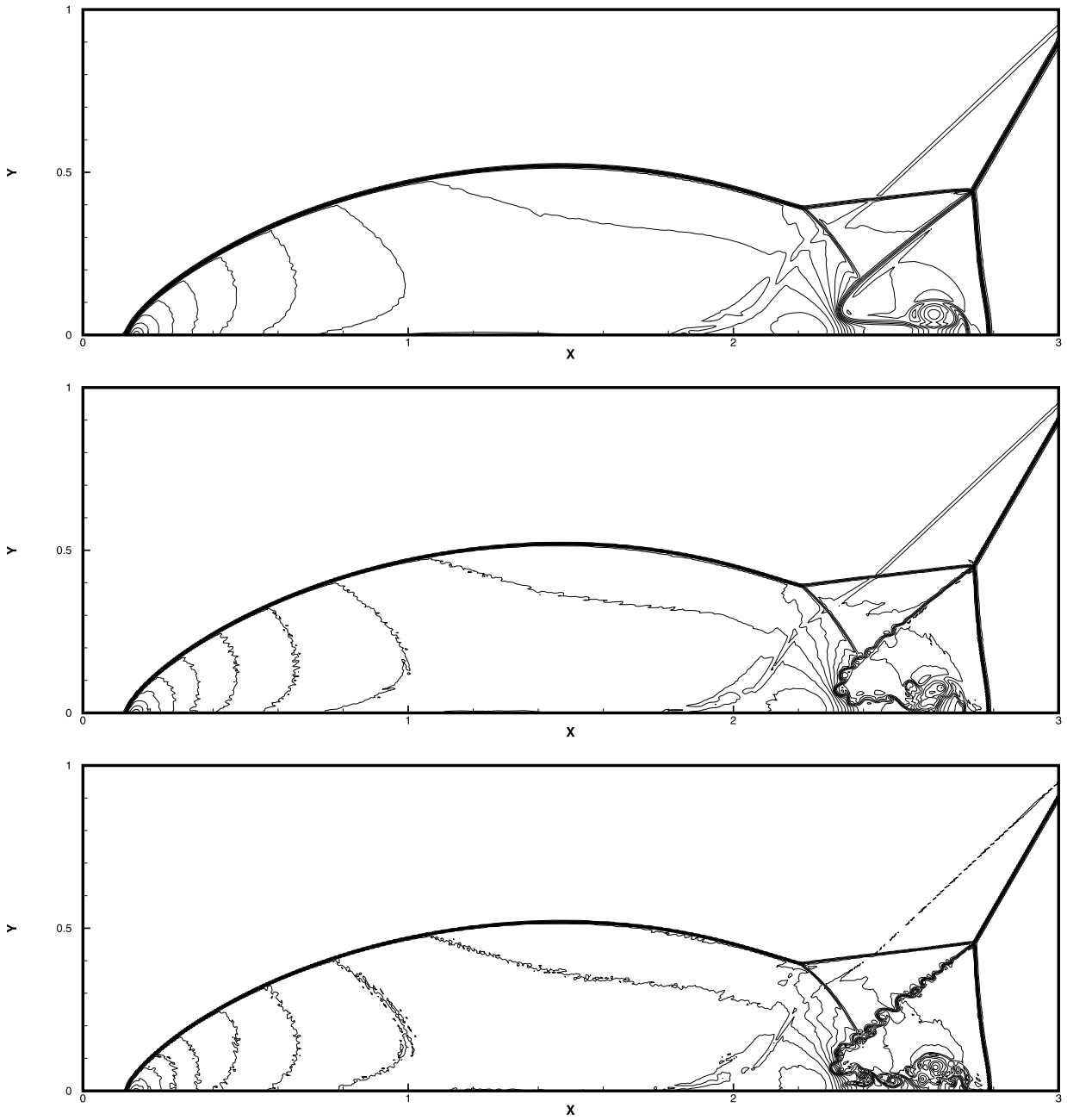

Fig. 4.9. Double Mach reflection problem. RKDG with new multi-resolution WENO limiter. Top: second-order ($k = 1$); middle: third-order ($k = 2$); bottom: fourth-order ($k = 3$). 30 equally spaced density contours from 1.5 to 21.5. The mesh points on the boundary are uniformly distributed with cell length $h = 1/200$.

Table 4.8
Forward step problem. The maximum and average percentages of troubled cells subject to the new multi-resolution WENO limiting.

	Percentage of the troubled cells							
P^1	cell length h	1/100	P^2	cell length h	1/100	P^3	cell length h	1/100
	maximum percent	3.16		maximum percent	10.3		maximum percent	9.25
	average percent	2.56		average percent	8.81		average percent	6.78

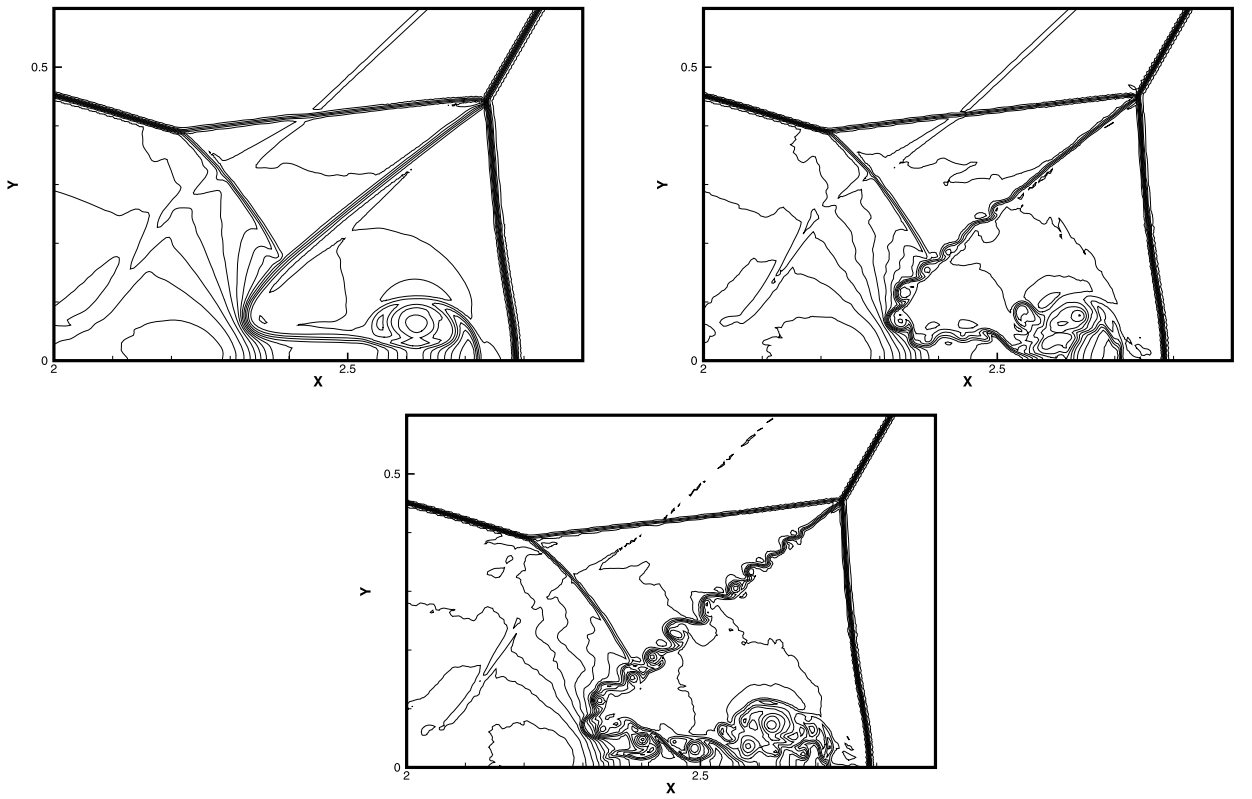

Fig. 4.10. Double Mach reflection problem. RKDG with new multi-resolution WENO limiter. Left: second-order ($k = 1$); right: third-order ($k = 2$); bottom: fourth-order ($k = 3$). Zoomed-in pictures around the Mach stem. 30 equally spaced density contours from 1.5 to 21.5. The mesh points on the boundary are uniformly distributed with cell length $h = 1/200$.

examples where the time step is smaller so as to guarantee that the spatial error dominates. We perform the new multi-resolution WENO limiting procedure on every triangular cell for simulating the accuracy tests, in order to fully testify the influence of the limiter upon accuracy. But we only define all triangular cells as troubled cells in Example 4.1 and Example 4.2, and will set the constant $C_k = 1$ in (3.1) in other examples, unless specified otherwise. We also set the linear weights as $\gamma_{\ell-1,\ell} = 0.01$ and $\gamma_{\ell,\ell} = 0.99$, $\ell = 1, 2, 3$, respectively, for simplicity in this paper.

Example 4.1. We first compute two-dimensional scalar Burgers' equation

$$u_t + \left(\frac{u^2}{2}\right)_x + \left(\frac{u^2}{2}\right)_y = 0, (x, y) \in [-2, 2] \times [-2, 2], \tag{4.1}$$

with the initial condition $u(x, y, 0) = 0.5 + \sin(\pi(x + y)/2)$ and periodic boundary conditions in both directions. The final time is $t = 0.5/\pi$, when the solution is still smooth. For this accuracy test case, the sample mesh is shown in Fig. 4.1. In order to fully test the effect of the new multi-resolution WENO limiter on accuracy, we perform the new limiting procedure on every triangular cell inside the computational domain. The L^1, L^∞, L^2 errors, and numerical orders of accuracy for the RKDG methods with/without new multi-resolution WENO limiters are shown in Table 4.1. It is observed that the new multi-resolution WENO limiters maintain the designed order of accuracy.

Example 4.2. We solve two-dimensional Euler equations (3.16). The computational field is [0,2] × [0,2]. The initial conditions are: $\rho(x, y, 0) = 1 + 0.2\sin(\pi(x + y))$, $\mu(x, y, 0) = 0.7$, $\nu(x, y, 0) = 0.3$, and $p(x, y, 0) = 1$. Periodic boundary conditions are applied in both directions. The exact solution of density is $\rho(x, y, t) = 1 + 0.2\sin(\pi(x + y - t))$. The final time is $t = 2$. For this test case, the sample mesh is shown in Fig. 4.2. Similar to the previous example, we define all triangular cells in the computational field as troubled cells and perform the new multi-resolution WENO limiting procedure on every triangular cell. The L^1, L^∞, L^2 errors, and numerical orders of accuracy of the density for the RKDG methods with new multi-resolution WENO limiters comparing with the original RKDG methods without limiters are shown in Table 4.2. Similar to the previous

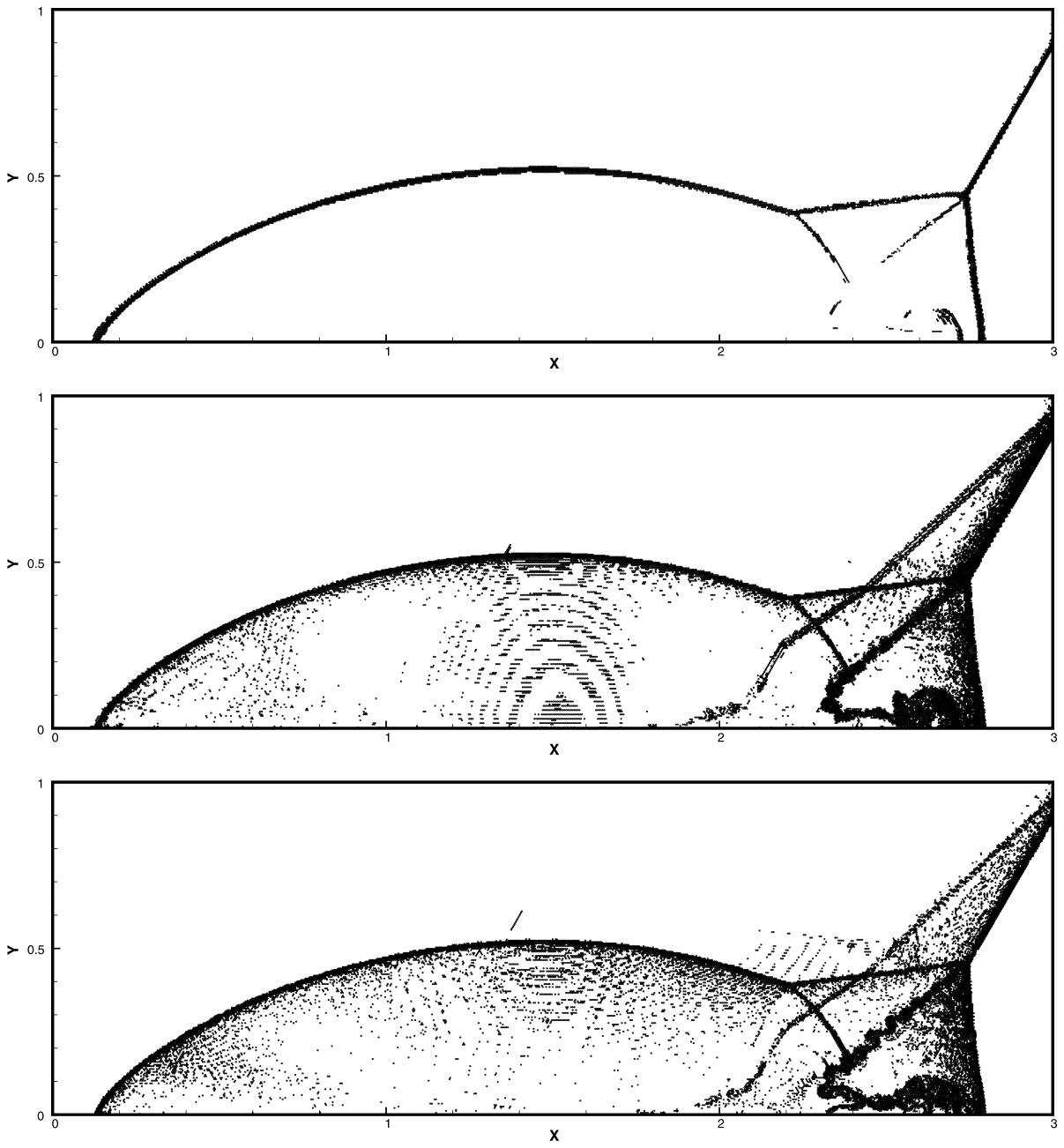

Fig. 4.11. Double Mach reflection problem. RKDG with new multi-resolution WENO limiter. Top: second-order ($k = 1$); middle: third-order ($k = 2$); bottom: fourth-order ($k = 3$). Troubled cells. Circles denote triangles which are identified as troubled cells subject to the new multi-resolution WENO limiting at the last time step. The mesh points on the boundary are uniformly distributed with cell length $h = 1/200$.

example, the new multi-resolution WENO limiting procedure can maintain the desired order of accuracy even though the cells in smooth regions are all "intentionally" identified as troubled cells.

Example 4.3. We solve the nonlinear Burgers' equation (4.1) with the same computational field $[-2, 2] \times [-2, 2]$ and the same initial condition $u(x, y, 0) = 0.5 + \sin(\pi(x + y)/2)$, except that we plot the results at $t = 1.5/\pi$ when a shock has already appeared in the solution. The solutions with the constant $C_k = 1$ in the troubled cell indicator, and when all cells are defined as troubled cells in the computational field, are shown in Fig. 4.3 for comparisons. We can see different RKDG methods with new multi-resolution WENO limiters could give non-oscillatory shock transitions for this problem in either case.

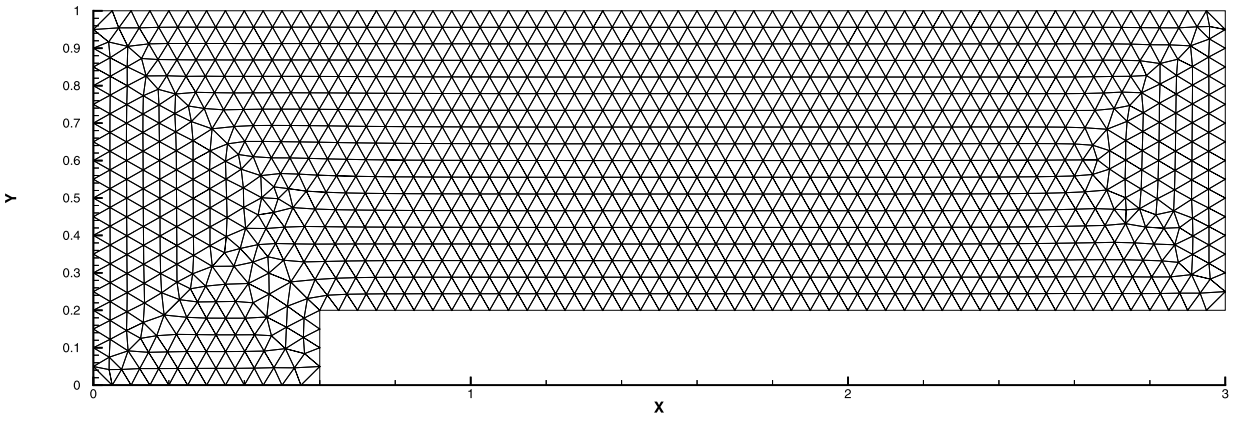

Fig. 4.12. Forward step problem. Sample mesh.

Example 4.4. We solve two-dimensional Euler equations (3.16) with the Riemann initial condition for the Lax problem [25]:

$$(\rho, \mu, \nu, p)^T = \begin{cases} (0.445, 0.698, 0, 3.528)^T, & x \in [-0.5, 0), \\ (0.5, 0, 0, 0.571)^T, & x \in [0, 0.5]. \end{cases} \tag{4.2}$$

The final time is $t = 0.16$. We seek the solution in the domain of $[-0.5, 0.5] \times [-0.025, 0.025]$ with a triangulation of 201 vertices in the x-direction and 11 vertices in the y-direction. The periodic boundary condition is applied in the y-direction. The results and zoomed-in pictures for different RKDG methods with new multi-resolution WENO limiters are shown in Fig. 4.4. The percentage of triangular cells declared to be troubled cells for different RKDG methods with new multi-resolution WENO limiters is given in Table 4.3. We observe good computational results obtained by the associated multi-resolution WENO limiting procedure.

Example 4.5. We solve two-dimensional Euler equations (3.16) with Riemann initial condition for the Sod problem [42]:

$$(\rho, \mu, \nu, p)^T = \begin{cases} (1, 0, 0, 2.5)^T, & x \in [-5, 0), \\ (0.125, 0, 0, 0.25)^T, & x \in [0, 5]. \end{cases} \tag{4.3}$$

The final time is $t = 2$. We seek the solution in the domain of $[-5, 5] \times [-0.25, 0.25]$ with a triangulation of 201 vertices in the x-direction and 11 vertices in the y-direction. The periodic boundary condition is applied in the y-direction. The results and zoomed-in pictures for associated methods are shown in Fig. 4.5. The percentage of triangular cells declared to be troubled cells for different RKDG methods with new multi-resolution WENO limiters is given in Table 4.4. The numerical results computed by RKDG methods with new multi-resolution WENO limiters are again in good shape.

Example 4.6. A higher order scheme would show its advantage when the solution contains both shocks and complex smooth region structures. A typical example for this is the problem of shock interaction with entropy waves [37,41]. We solve two-dimensional Euler equations (3.16) with a moving Mach 3 shock interacting with sine waves in density in the x-direction: $(\rho, \mu, \nu, p)^T = (3.857143, 2.629369, 0, 10.333333)^T$ for $x \in [-5, -4)$; $(\rho, \mu, \nu, p)^T = (1 + 0.2\sin(5x), 0, 0, 1)^T$ for $x \in [-4, 5]$. The solution of the Euler equations (3.16) is obtained in the domain of $[-5, 5] \times [-0.25, 0.25]$ with a triangulation of 201 vertices in the x-direction and 11 vertices in the y-direction. The periodic boundary condition is applied in the y-direction. The computed density ρ is plotted at $t = 1.8$ against the reference "exact" solution which is a converged solution computed by the finite difference fifth-order WENO scheme [23] with 2000 grid points in Fig. 4.6. The percentage of triangular cells declared to be troubled cells for different RKDG methods with new multi-resolution WENO limiters is given in Table 4.5. The second-order, third-order, and fourth-order RKDG methods with new multi-resolution WENO limiters could get good resolution for this example, and we can clearly observe increased resolution for higher order RKDG methods.

Example 4.7. We now consider the interaction of two blast waves [43]. The initial condition is:

$$(\rho, \mu, \nu, p)^T = \begin{cases} (1, 0, 0, 10^3)^T, & 0 < x < 0.1, \\ (1, 0, 0, 10^{-2})^T, & 0.1 < x < 0.9, \\ (1, 0, 0, 10^2)^T, & 0.9 < x < 1. \end{cases} \tag{4.4}$$

The computed density ρ is plotted at $t = 0.038$ against the reference "exact" solution which is a converged solution computed by the finite difference fifth-order WENO scheme [23] with 20000 grid points. The solution of the Euler equations

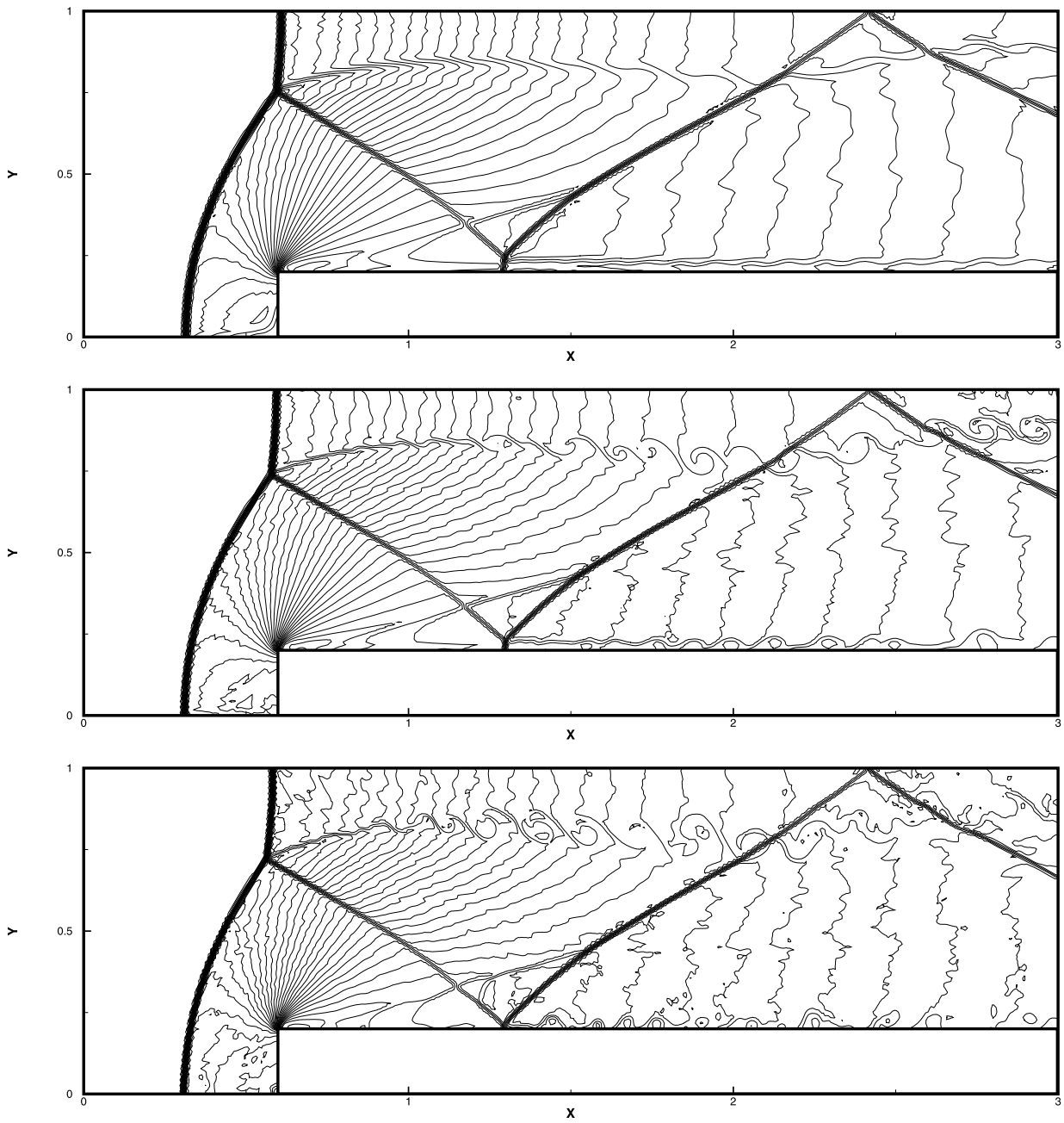

Fig. 4.13. Forward step problem. RKDG with new multi-resolution WENO limiter. Top: second-order ($k = 1$); middle: third-order ($k = 2$); bottom: fourth-order ($k = 3$). 30 equally spaced density contours from 0.32 to 6.15. The mesh points on the boundary are uniformly distributed with cell length $h = 1/100$.

(3.16) is obtained in the domain of $[0, 1] \times [-0.0125, 0.0125]$ with a triangulation of 401 vertices in the x-direction and 11 vertices in the y-direction. The periodic boundary condition is applied in the y-direction. The results and zoomed in pictures for different RKDG methods are shown in Fig. 4.7. The percentage of triangular cells declared to be troubled cells for different RKDG methods with new multi-resolution WENO limiters is given in Table 4.6. The new multi-resolution WENO limiting procedure could get good performance as before, with increased resolution for higher order accuracy.

Example 4.8. Double Mach reflection problem. This model problem is originally from [43]. We solve the Euler equations (3.16) in a computational domain of $[0, 4] \times [0, 1]$. The reflection boundary condition is used at the wall, while for the rest of the bottom boundary (the part from $x = 0$ to $x = \frac{1}{6}$), and the exact post-shock condition is imposed. At the top boundary is the exact motion of the Mach 10 shock. The results shown are at $t = 0.2$. Three different orders of accuracy for the

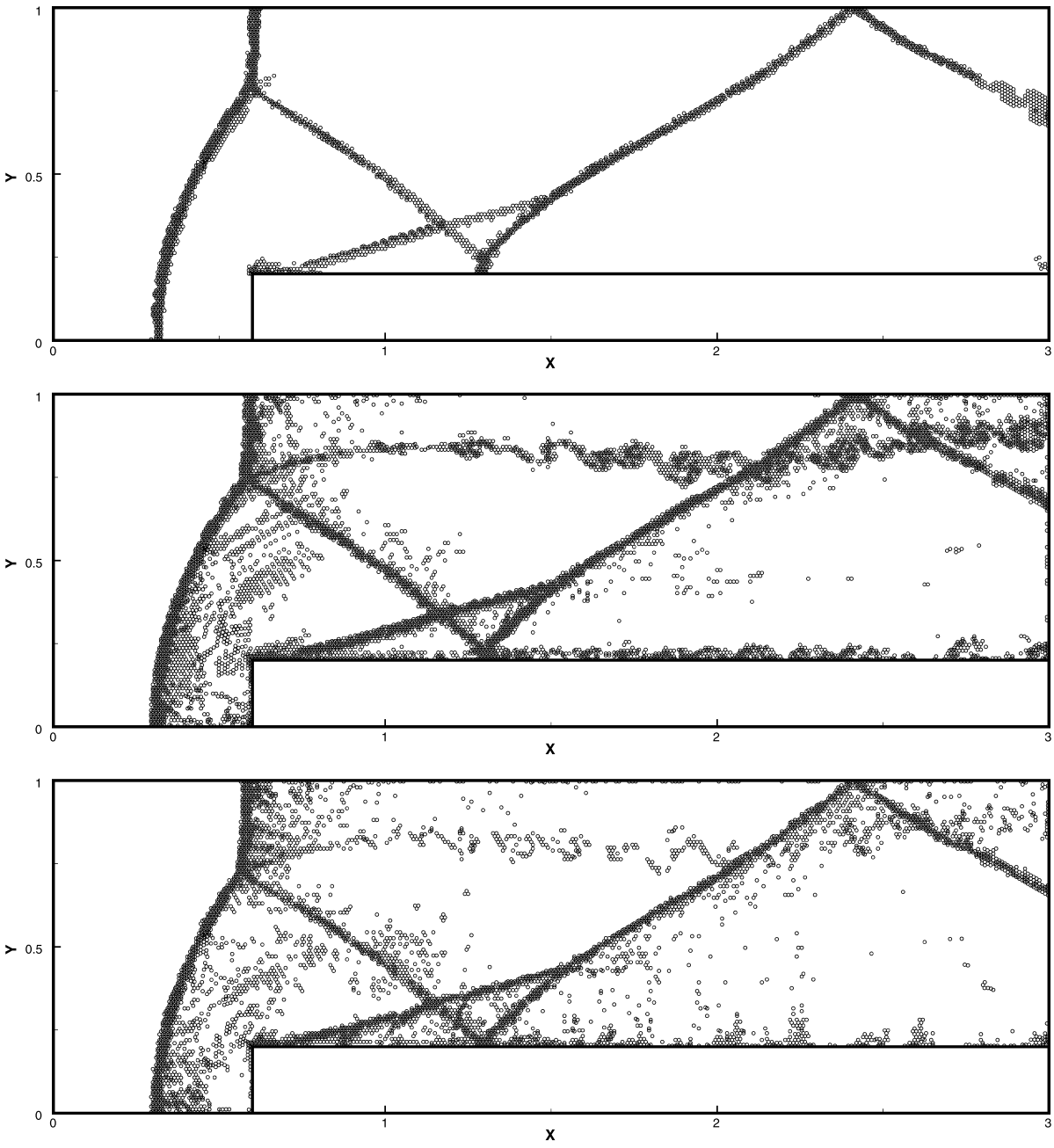

Fig. 4.14. Forward step problem. RKDG with new multi-resolution WENO limiter. Top: second-order ($k = 1$); middle: third-order ($k = 2$); bottom: fourth-order ($k = 3$). Troubled cells. Circles denote triangles which are identified as troubled cells subject to the new multi-resolution WENO limiting at the last time step. The mesh points on the boundary are uniformly distributed with cell length $h = 1/100$.

RKDG methods with new multi-resolution WENO limiters, $k = 1$, $k = 2$, and $k = 3$ (second-order, third-order, and fourth-order accuracies), are used in this two-dimensional example. A sample mesh is shown in Fig. 4.8. The simulation results are shown in Fig. 4.9. The "zoomed-in" pictures around the double Mach stem to show more details are given in Fig. 4.10. The percentage of triangular cells declared to be troubled cells for different RKDG methods with new multi-resolution WENO limiters is given in Table 4.7. The troubled cells identified at the last time step are shown in Fig. 4.11. Clearly, the resolution improves with an increasing k on the same mesh level.

Example 4.9. A Mach 3 wind tunnel with a step. This model problem is also originally from [43]. The setup of the problem is as follows. The wind tunnel is one length unit wide and three length units long. The step is 0.2 length units high and is located 0.6 length units from the left-hand end of the tunnel. The problem is initialized by a right-going Mach 3 flow.

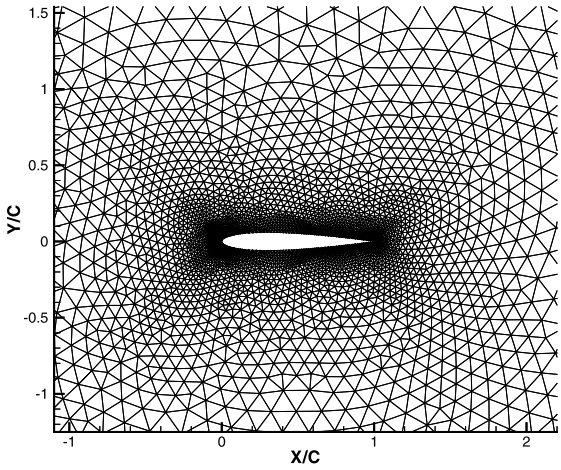

Fig. 4.15. NACA0012 airfoil mesh. Zoomed-in mesh.

Table 4.9
NACA0012 airfoil problem. The maximum and average percentages of troubled cells subject to the new multi-resolution WENO limiting.

	$M_\infty = 0.8$, angle of attack $\alpha = 1.25°$		$M_\infty = 0.85$, angle of attack $\alpha = 1°$	
P^1	maximum percentage	2.17	maximum percentage	2.24
	average percentage	0.73	average percentage	1.26
P^2	maximum percentage	5.66	maximum percentage	5.80
	average percentage	2.55	average percentage	3.41
P^3	maximum percentage	4.86	maximum percentage	5.07
	average percentage	2.43	average percentage	3.91

Reflective boundary conditions are applied along the wall of the tunnel and inflow/outflow boundary conditions are applied at the entrance/exit. The results are shown at $t = 4$. We present a sample triangulation of the whole region $[0, 3] \times [0, 1]$ in Fig. 4.12. In Fig. 4.13, we show 30 equally spaced density contours from 0.32 to 6.15 computed by the second-order, third-order, and fourth-order RKDG methods with new multi-resolution WENO limiters, respectively. The percentage of triangular cells declared to be troubled cells for different RKDG methods with new multi-resolution WENO limiters is given in Table 4.8. The troubled cells identified at the last time step are shown in Fig. 4.14. We can clearly observe that the fourth-order scheme gives better resolution than the second-order and third-order schemes, especially for the resolution of the physical instability and roll-up of the contact line.

Example 4.10. We consider inviscid Euler transonic flow past a single NACA0012 airfoil configuration with Mach number $M_\infty = 0.8$, angle of attack $\alpha = 1.25°$, and with $M_\infty = 0.85$, angle of attack $\alpha = 1°$. The computational domain is $[-15, 15] \times [-15, 15]$. The mesh used in the computation is shown in Fig. 4.15, consisting of 9340 elements with the maximum diameter of the circumcircle being 1.4188 and the minimum diameter being 0.0031 near the airfoil. The mesh uses curved cells near the airfoil. The second-order, third-order, and fourth-order RKDG methods with new multi-resolution WENO limiters are used in the numerical experiment. Mach number distributions are shown in Fig. 4.16. Fig. 4.17 shows the pressure (C_p) distributions on each cell-face for solutions obtained by second-order, third-order, and fourth-order RKDG methods with new multi-resolution WENO limiters, respectively. The percentage of triangular cells declared to be troubled cells for different RKDG methods with new multi-resolution WENO limiters is given in Table 4.9. The troubled cells identified at the last time step are shown in Fig. 4.18 and very few cells are identified as troubled cells with the application of new modified version of the original KXRCF shock detection technique [24].

5. Concluding remarks

We have designed a new type of multi-resolution WENO limiters for the second-order, third-order, and fourth-order Runge-Kutta discontinuous Galerkin (RKDG) methods for solving two-dimensional scalar equation and hyperbolic conservation laws on triangular meshes. The general framework of such multi-resolution WENO limiters for high-order RKDG methods is to modify a new version of the original KXRCF shock detection technique [24] to detect troubled cells subject to

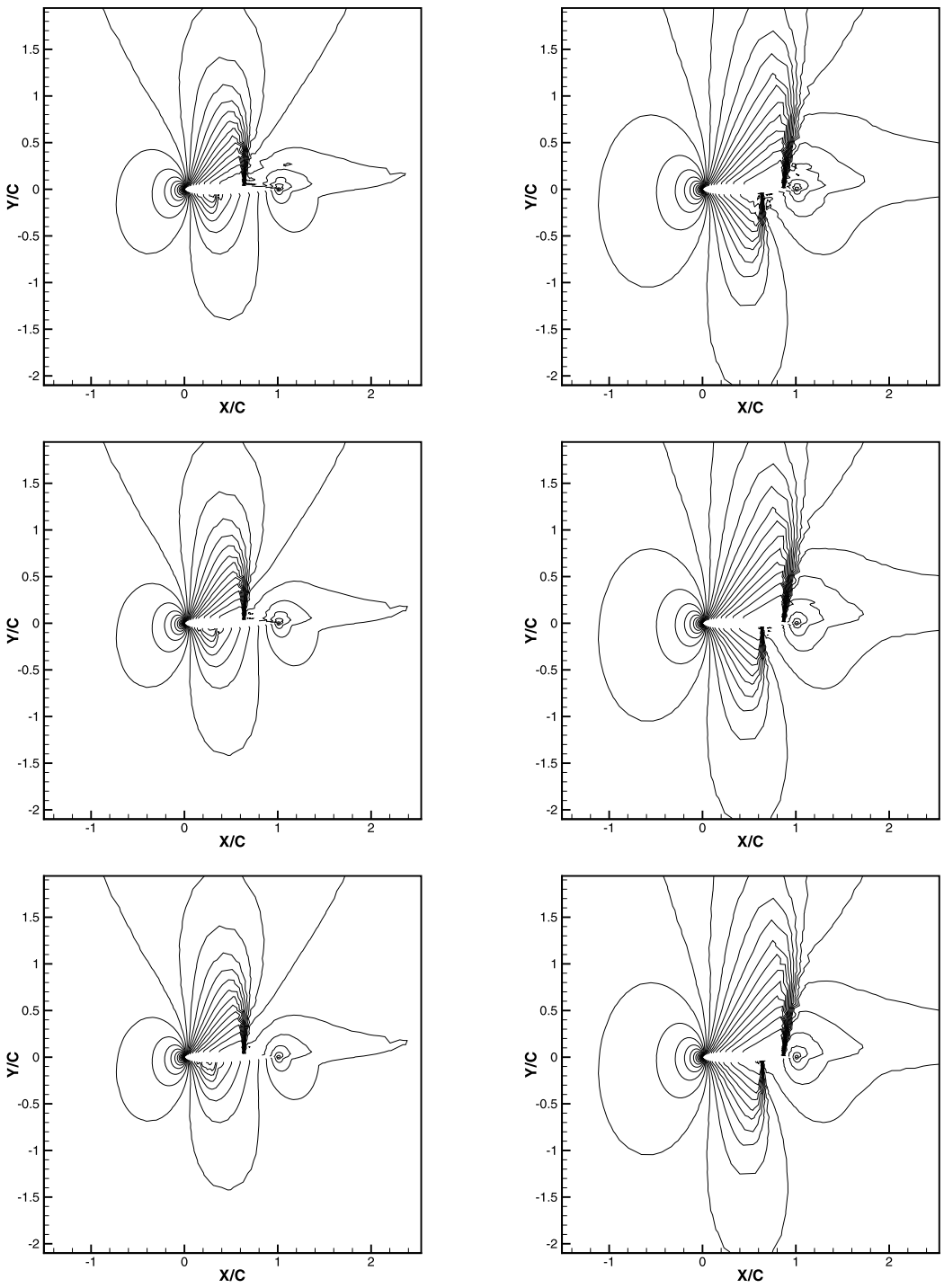

Fig. 4.16. NACA0012 airfoil. RKDG with new multi-resolution WENO limiter. Top: second-order ($k = 1$); middle: third-order ($k = 2$); bottom: fourth-order ($k = 3$). Mach number. Left: $M_\infty = 0.8$, angle of attack $\alpha = 1.25°$, 30 equally spaced Mach number contours from 0.172 to 1.325; right: $M_\infty = 0.85$, angle of attack $\alpha = 1°$, 30 equally spaced Mach number contours from 0.158 to 1.357.

the multi-resolution WENO limiting procedure on triangular meshes, and construct a sequence of hierarchical L^2 projection polynomial solutions of the DG methods over the troubled cell. The main innovation is the new multi-resolution WENO reconstruction procedure, which basically only uses the information defined within the triangular troubled cell, with information from neighboring triangular cells used marginally in the determination of the smoothness indicator of the lowest

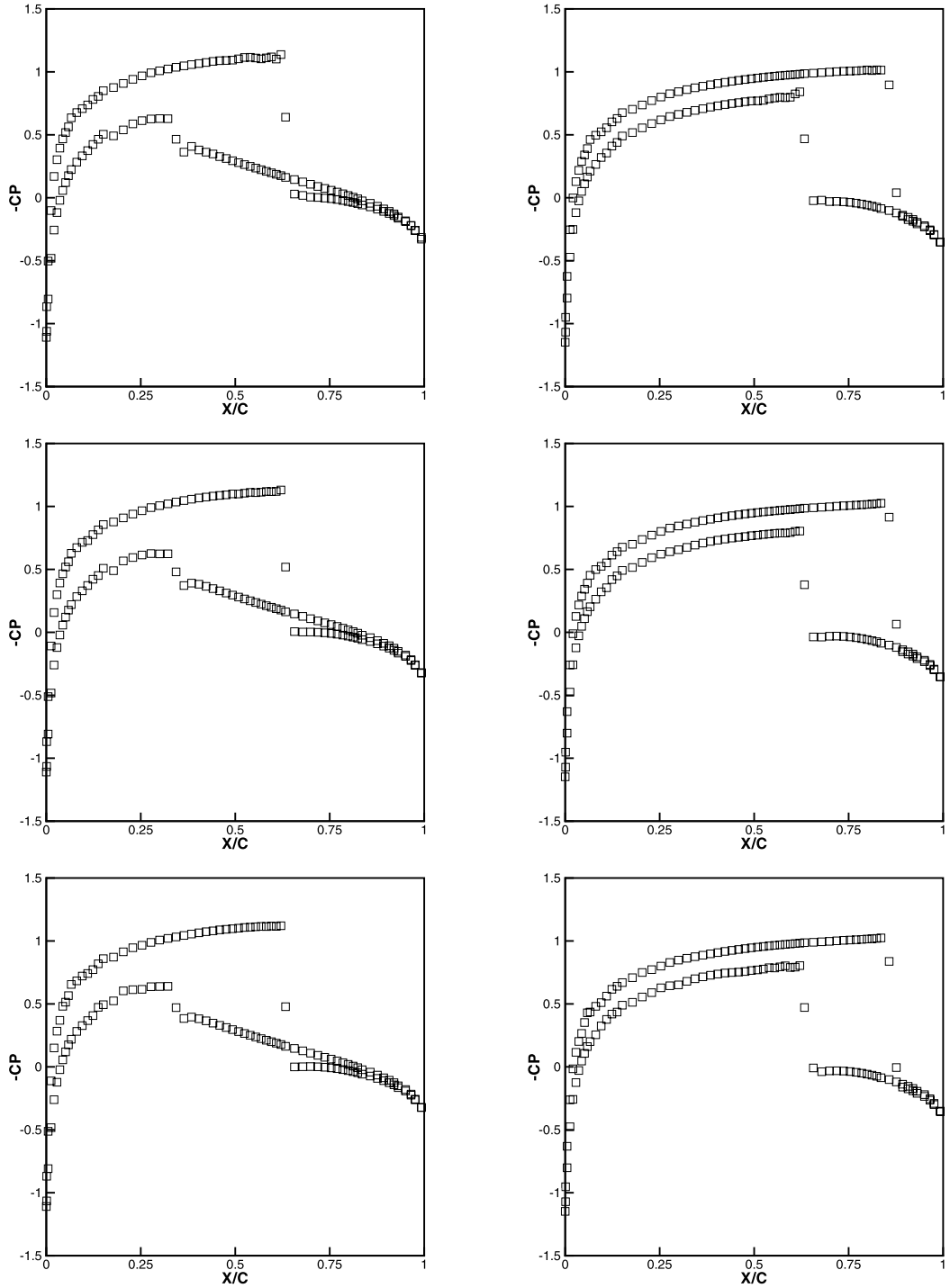

Fig. 4.17. NACA0012 airfoil. RKDG with new multi-resolution WENO limiter. Top: second-order ($k = 1$); middle: third-order ($k = 2$); bottom: fourth-order ($k = 3$). Pressure distribution. Left: $M_\infty = 0.8$, angle of attack $\alpha = 1.25°$; right: $M_\infty = 0.85$, angle of attack $\alpha = 1°$.

order polynomial in the hierarchy, and with simple positive linear weights in the spatial reconstruction procedure. This new spatial reconstruction methodology is simpler, more robust, and could lead to better resolutions for standard test examples than previous WENO type limiters for the RKDG methods on triangular meshes. The framework of these multi-resolution WENO limiters for arbitrary high-order RKDG methods would also be very simple on three-dimensional tetrahedral meshes and the study of which is our ongoing work.

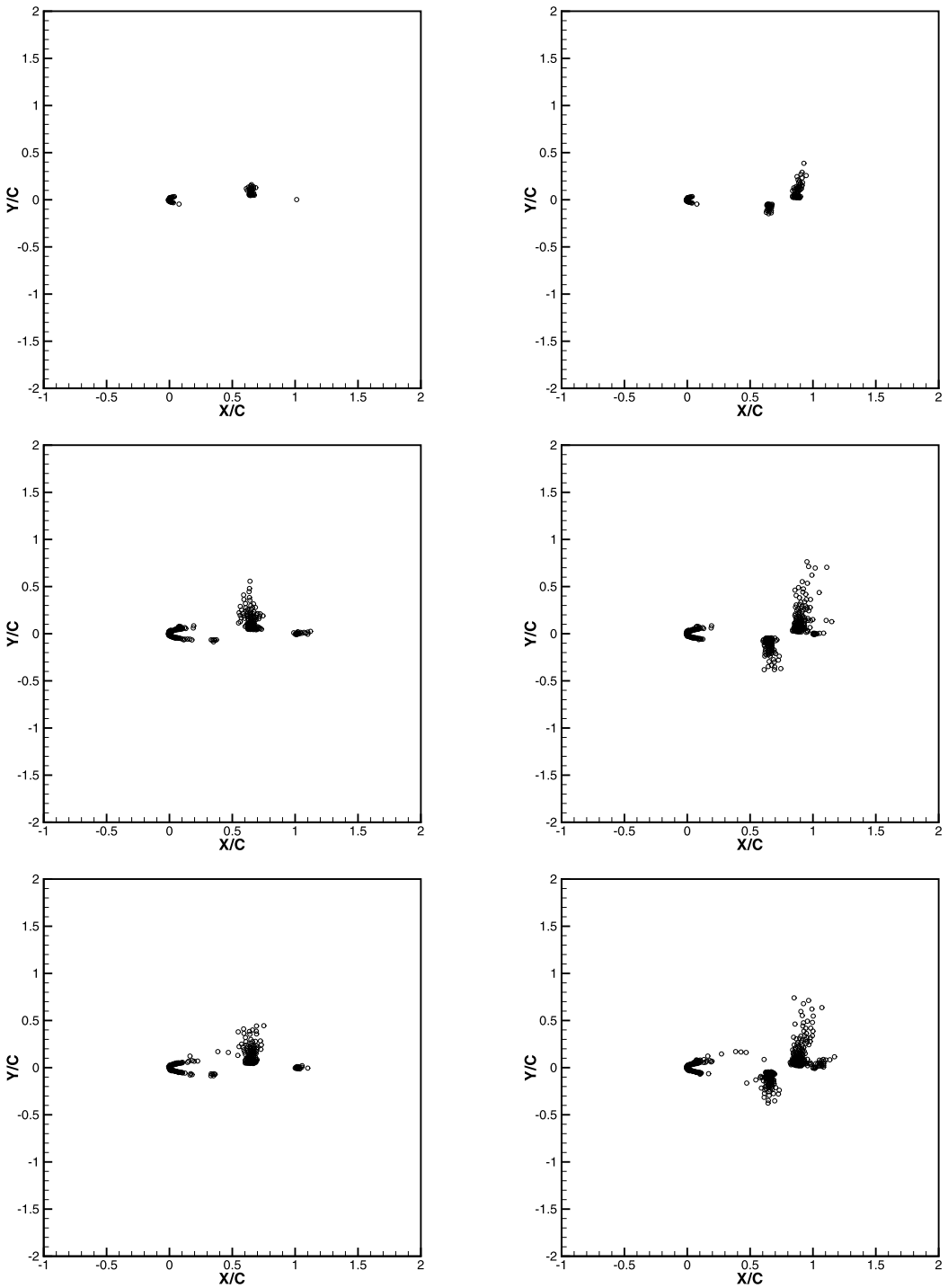

Fig. 4.18. NACA0012 airfoil. RKDG with new multi-resolution WENO limiter. Top: second-order ($k = 1$); middle: third-order ($k = 2$); bottom: fourth-order ($k = 3$). Troubled cells. Circles denote triangles which are identified as troubled cells subject to the new multi-resolution WENO limiting at the last time step. Left: $M_\infty = 0.8$, angle of attack $\alpha = 1.25°$; right: $M_\infty = 0.85$, angle of attack $\alpha = 1°$.

References

[1] R. Biswas, K.D. Devine, J. Flaherty, Parallel, adaptive finite element methods for conservation laws, Appl. Numer. Math. 14 (1994) 255–283.

[2] R. Borges, M. Carmona, B. Costa, W.S. Don, An improved weighted essentially non-oscillatory scheme for hyperbolic conservation laws, J. Comput. Phys. 227 (2008) 3191–3211.

[3] A. Burbeau, P. Sagaut, C.H. Bruneau, A problem-independent limiter for high-order Runge-Kutta discontinuous Galerkin methods, J. Comput. Phys. 169 (2001) 111–150.
[4] G. Capdeville, A central WENO scheme for solving hyperbolic conservation laws on non-uniform meshes, J. Comput. Phys. 227 (2008) 2977–3014.
[5] M. Castro, B. Costa, W.S. Don, High order weighted essentially non-oscillatory WENO-Z schemes for hyperbolic conservation laws, J. Comput. Phys. 230 (2011) 1766–1792.
[6] B. Cockburn, Discontinuous Galerkin methods for convection-dominated problems, in: T. Barth, H. Deconinck (Eds.), High-Order Methods for Computational Physics, in: Lecture Notes in Computational Science and Engineering, vol. 9, Springer, Berlin, 1999, pp. 69–224.
[7] B. Cockburn, S. Hou, C.-W. Shu, The Runge-Kutta local projection discontinuous Galerkin finite element method for conservation laws IV: the multidimensional case, Math. Comput. 54 (1990) 545–581.
[8] B. Cockburn, S.-Y. Lin, C.-W. Shu, TVB Runge-Kutta local projection discontinuous Galerkin finite element method for conservation laws III: one dimensional systems, J. Comput. Phys. 84 (1989) 90–113.
[9] B. Cockburn, C.-W. Shu, TVB Runge-Kutta local projection discontinuous Galerkin finite element method for conservation laws II: general framework, Math. Comput. 52 (1989) 411–435.
[10] B. Cockburn, C.-W. Shu, The Runge-Kutta local projection P1-discontinuous Galerkin finite element method for scalar conservation laws, RAIRO Modél. Math. Anal. Numér. 25 (1991) 337–361.
[11] B. Cockburn, C.-W. Shu, The Runge-Kutta discontinuous Galerkin method for conservation laws V: multidimensional systems, J. Comput. Phys. 141 (1998) 199–224.
[12] B. Cockburn, C.-W. Shu, Runge-Kutta discontinuous Galerkin method for convection-dominated problems, J. Sci. Comput. 16 (2001) 173–261.
[13] M. Dumbser, M. Käser, Arbitrary high order non-oscillatory finite volume schemes on unstructured meshes for linear hyperbolic systems, J. Comput. Phys. 221 (2007) 693–723.
[14] O. Friedrichs, Weighted essentially non-oscillatory schemes for the interpolation of mean values on unstructured grids, J. Comput. Phys. 144 (1998) 194–212.
[15] G. Fu, C.-W. Shu, A new troubled-cell indicator for discontinuous Galerkin methods for hyperbolic conservation laws, J. Comput. Phys. 347 (2017) 305–327.
[16] A. Harten, Multi-resolution analysis for ENO schemes, Institute for Computer Applications in Science and Engineering, NASA Langley Research Center, Hampton, Virginia, September 1991 23665-5225, Contract No. NAS1-18605.
[17] A. Harten, Discrete multi-resolution analysis and generalized wavelets, Appl. Numer. Math. 12 (1993) 153–192.
[18] A. Harten, Adaptive multiresolution schemes for shock computations, Comput. Phys. 115 (1994) 319–338.
[19] A. Harten, Multiresolution algorithms for the numerical solution of hyperbolic conservation laws, Commun. Pure Appl. Math. 48 (1995) 1305–1342.
[20] A. Harten, Multiresolution representation of data: a general framework, SIAM J. Numer. Anal. 33 (1996) 1205–1256.
[21] J. Hesthaven, T. Warburton, Nodal Discontinuous Galerkin Methods, Springer, New York, 2008.
[22] C. Hu, C.-W. Shu, Weighted essentially non-oscillatory schemes on triangular meshes, J. Comput. Phys. 150 (1999) 97–127.
[23] G. Jiang, C.-W. Shu, Efficient implementation of weighted ENO schemes, J. Comput. Phys. 126 (1996) 202–228.
[24] L. Krivodonova, J. Xin, J.-F. Remacle, N. Chevaugeon, J.E. Flaherty, Shock detection and limiting with discontinuous Galerkin methods for hyperbolic conservation laws, Appl. Numer. Math. 48 (2004) 323–338.
[25] P.D. Lax, Weak solutions of nonlinear hyperbolic equations and their numerical computation, Commun. Pure Appl. Math. 7 (1954) 159–193.
[26] D. Levy, G. Puppo, G. Russo, Central WENO schemes for hyperbolic systems of conservation laws, M2AN Math. Model. Numer. Anal. 33 (1999) 547–571.
[27] D. Levy, G. Puppo, G. Russo, Compact central WENO schemes for multidimensional conservation laws, SIAM J. Sci. Comput. 22 (2) (2000) 656–672.
[28] B. Li, Discontinuous Finite Elements in Fluid Dynamics and Heat Transfer, Birkhauser, Basel, 2006.
[29] X. Liu, S. Osher, T. Chan, Weighted essentially non-oscillatory schemes, J. Comput. Phys. 115 (1994) 200–212.
[30] H. Luo, J.D. Baum, R. Lohner, A Hermite WENO-based limiter for discontinuous Galerkin method on unstructured grids, J. Comput. Phys. 225 (2007) 686–713.
[31] H. Luo, J.D. Baum, R. Lohner, On the computation of steady-state compressible flows using a discontinuous Galerkin method, Int. J. Numer. Methods Eng. 73 (2008) 597–623.
[32] J. Qiu, C.-W. Shu, Hermite WENO schemes and their application as limiters for Runge-Kutta discontinuous Galerkin method: one dimensional case, J. Comput. Phys. 193 (2003) 115–135.
[33] J. Qiu, C.-W. Shu, Runge-Kutta discontinuous Galerkin method using WENO limiters, SIAM J. Sci. Comput. 26 (2005) 907–929.
[34] J. Qiu, C.-W. Shu, A comparison of troubled-cell indicators for Runge-Kutta discontinuous Galerkin methods using weighted essentially nonoscillatory limiters, SIAM J. Sci. Comput. 27 (2005) 995–1013.
[35] J. Qiu, C.-W. Shu, Hermite WENO schemes and their application as limiters for Runge-Kutta discontinuous Galerkin method II: two dimensional case, Comput. Fluids 34 (2005) 642–663.
[36] W.H. Reed, T.R. Hill, Triangular mesh methods for the neutron transport equation, Tech. Report LA-UR-73-479, Los Alamos Scientific Laboratory, Los Alamos, NM, 1973.
[37] C.-W. Shu, Essentially non-oscillatory and weighted essentially non-oscillatory schemes for hyperbolic conservation laws, in: A. Quarteroni (Ed.), Advanced Numerical Approximation of Nonlinear Hyperbolic Equations, B. Cockburn, C. Johnson, C.-W. Shu and E. Tadmor, in: Lecture Notes in Mathematics, vol. 1697, Springer, 1998, pp. 325–432.
[38] C.-W. Shu, Discontinuous Galerkin methods: general approach and stability, in: Numerical Solutions of Partial Differential Equations, S. Bertoluzza, S. Falletta, G. Russo and C.-W. Shu, Advanced Courses in Mathematics CRM Barcelona, Birkhäuser, Basel, 2009, pp. 149–201.
[39] C.-W. Shu, High order weighted essentially non-oscillatory schemes for convection dominated problems, SIAM Rev. 51 (2009) 82–126.
[40] C.-W. Shu, S. Osher, Efficient implementation of essentially non-oscillatory shock-capturing schemes, J. Comput. Phys. 77 (1988) 439–471.
[41] C.-W. Shu, S. Osher, Efficient implementation of essentially non-oscillatory shock capturing schemes II, J. Comput. Phys. 83 (1989) 32–78.
[42] G. Sod, A survey of several finite difference methods for systems of nonlinear hyperbolic conservation laws, J. Comput. Phys. 27 (1978) 1–31.
[43] P. Woodward, P. Colella, The numerical simulation of two-dimensional fluid flow with strong shocks, J. Comput. Phys. 54 (1984) 115–173.
[44] X. Zhong, C.-W. Shu, A simple weighted essentially nonoscillatory limiter for Runge-Kutta discontinuous Galerkin methods, J. Comput. Phys. 232 (2013) 397–415.
[45] J. Zhu, J. Qiu, A new fifth order finite difference WENO scheme for solving hyperbolic conservation laws, J. Comput. Phys. 318 (2016) 110–121.
[46] J. Zhu, J. Qiu, A new type of finite volume WENO schemes for hyperbolic conservation laws, J. Sci. Comput. 73 (2017) 1338–1359.
[47] J. Zhu, J. Qiu, C.-W. Shu, High-order Runge-Kutta discontinuous Galerkin methods with a new type of multi-resolution WENO limiters, J. Comput. Phys. 404 (2020) 109105.
[48] J. Zhu, J. Qiu, C.-W. Shu, M. Dumbser, Runge-Kutta discontinuous Galerkin method using WENO limiters II: unstructured meshes, J. Comput. Phys. 227 (2008) 4330–4353.
[49] J. Zhu, C.-W. Shu, A new type of multi-resolution WENO schemes with increasingly higher order of accuracy, J. Comput. Phys. 375 (2018) 659–683.
[50] J. Zhu, C.-W. Shu, A new type of multi-resolution WENO schemes with increasingly higher order of accuracy on triangular meshes, J. Comput. Phys. 392 (2019) 19–33.

[51] J. Zhu, C.-W. Shu, A new type of third-order finite volume multi-resolution WENO schemes on tetrahedral meshes, J. Comput. Phys. 406 (2020) 109212.
[52] J. Zhu, X. Zhong, C.-W. Shu, J. Qiu, Runge-Kutta discontinuous Galerkin method using a new type of WENO limiters on unstructured meshes, J. Comput. Phys. 248 (2013) 200–220.
[53] J. Zhu, X. Zhong, C.-W. Shu, J. Qiu, Runge-Kutta discontinuous Galerkin method with a simple and compact Hermite WENO limiter on unstructured meshes, Commun. Comput. Phys. 21 (2017) 623–649.